

# Post-Routing Arithmetic in Llama-3: Last-Token Result Writing and Rotation-Structured Digit Directions

Yao Yan

Chongqing Normal University  
Chongqing Key Lab of Cognitive Intelligence and Intelligent Finance  
Chongqing, China  
yaoyan@stu.cqnu.edu.cn

## Abstract

We study three-digit addition in Meta-Llama-3-8B (base) under a one-token read-out to characterize how arithmetic answers are finalized after cross-token routing becomes causally irrelevant. Causal residual patching and cumulative attention ablations localize a sharp boundary near layer 17: beyond it, the decoded sum is controlled almost entirely by the last input token and late-layer self-attention is largely dispensable. In this post-routing regime, digit(-sum) direction dictionaries vary with a next-higher-digit context but are well-related by an approximately orthogonal map inside a shared low-rank subspace (low-rank Procrustes alignment). Causal digit editing matches this geometry: naive cross-context transfer fails, while rotating directions through the learned map restores strict counterfactual edits; negative controls do not recover.

## 1 Introduction

Large language models (LLMs) solve multi-digit addition with near-perfect accuracy in-context, but we still lack a mechanistic account of how a decoder-only transformer finalizes an arithmetic answer once attention-based routing is no longer causally decisive. We ask: after routing ends, where is the answer represented, and what writes it into the next-token prediction?

We study three-digit addition in Meta-Llama-3-8B (base) using a deliberately simple read-out: prompts of the form "Calculate: {a}+{b} = " followed by greedy decoding of a single next token, parsed as an integer (Sec. 3). This one-token protocol makes causal localiza-

tion sharp and allows direct intervention tests on `resid_post`.

We find a sharp *result-writing boundary* near layer 16 (Sec. 4): cross-sample residual patching shifts causal control from non-last tokens to the last input token, and cumulative attention ablation indicates that self-attention is largely dispensable beyond this boundary. In the resulting post-routing regime, digit(-sum) direction dictionaries are strongly context-conditioned yet structured: across shifts in a next-higher-digit nuisance context, within-context dictionaries are related by an approximately orthogonal re-parameterization inside a shared low-rank core (Sec. 6). We causally validate the corresponding prediction: cross-context transfer of directions collapses, while applying the learned rotator restores strict counterfactual digit edits, with negative controls failing to recover (Sec. 7).

## Contributions.

- We causally localize a sharp result-writing boundary near layer 16 where three-digit addition becomes effectively last-token-only and late-layer attention is largely dispensable.
- We characterize a context-conditioned but rotation-like structure in digit(-sum) direction dictionaries, captured by low-rank Procrustes alignment in a shared low-rank core.
- We provide causal validation via strict counterfactual digit editing: rotated directions recover cross-context editability while transfer fails, and negative controls do not recover.

## 2 Related Work

**Arithmetic and algorithmic reasoning.** (Anthropic, 2025; Mamidanna et al., 2025; Nikankin et al., 2025; Quirke and Barez, 2024; Zhu et al.,

---

If this paper is accepted, we will release the code publicly.

2025) Mechanistic analyses of synthetic arithmetic often reveal structured internal algorithms and representations. (Stolfo et al., 2023; Zhou et al., 2024) Work on modular arithmetic characterizes Fourier-like mechanisms and attention-mediated computation (Nanda et al., 2023). For multi-digit addition, recent studies identify digit-wise structure and carry-related phenomena in transformer activations and circuits (Kruthoff, 2024; Quirke and Barez, 2024; Heimersheim and Nanda, 2024; Zhang and Nanda, 2024). We focus specifically on late-stage answer finalization in a large decoder-only LLM under a one-token readout.

**Causal interventions and activation editing.** Beyond correlational probing (Belinkov, 2022), causal methods intervene on activations via patching, mediation, and tracing (Stolfo et al., 2023; Lindsey et al., 2025). A complementary line studies low-dimensional functional directions as controllable edits (e.g., rank-one updates and steering vectors) (Meng et al., 2022; Arditì et al., 2024; Chan et al., 2022). We combine these ideas to analyze a post-routing last-token regime and show that context-dependent direction families are related by low-rank orthogonal alignment.

### 3 Experimental Setup

**Task distribution.** We study three-digit addition with operands sampled uniformly from  $a, b \in \{1, \dots, 999\}$ . Unless stated otherwise, we restrict to instances whose gold sum  $s = a + b$  lies in  $[200, 999]$  so the result is a three-digit integer and matches our one-token numeric readout.

**Prompt templates.** Our default prompt is "Calculate: {a}+{b} = " (note the trailing space).

**Model and activations.** We use Meta-Llama-3-8B (base) (Dubey et al., 2024) in BF16 without quantization. Interventions operate on transformer-block outputs (`resid_post`). Throughout, "layer  $l$ " refers to the output of block  $l \in \{1, \dots, 32\}$ .

**One-token readout and parsing.** We append a trailing space in the prompt so that the answer begins at a fresh token boundary. With the Meta-Llama-3 tokenizer used in our experiments, every base-10 integer in  $[0, 1000]$  (in the whitespace-prefixed form induced by our template) is repre-

sented as a single token; accordingly, we greedily decode exactly the first next token and treat it as the model’s numeric answer.

**Baseline and evaluation convention.** By default we report baseline (no-intervention) performance on the same evaluation distribution; baseline strict accuracy is typically  $\approx 99\%$  under this one-token protocol. When an experiment conditions on baseline correctness (e.g., for scale selection), we state it explicitly.

## 4 Causal Localization of the Result-Writing Boundary

All later experiments assume a *post-routing last-token regime* in which (i) the decoded arithmetic result is causally controlled by the last input token’s residual stream and (ii) late-layer self-attention is no longer necessary. (Mamidanna et al., 2025) We establish this regime with two targeted causal tests at `resid_post` under the one-token readout (Sec. 3): **(1) cross-sample residual patching**, which asks *where* result semantics are stored, and **(2) cumulative attention ablation**, which asks whether attention is still required once the boundary is reached. Implementation details, per-layer curves, and auxiliary diagnostics are deferred to Appendix A.

### 4.1 Cross-sample residual patching localizes answer semantics

We form baseline-correct source–target prompt pairs and patch `resid_post` at a chosen layer  $L$  by overwriting either (i) the last-token row only (*last-token patch*) or (ii) all non-last rows (*non-last patch*), then decode the single next token and parse it as an integer (Sec. 3) (Zhang and Nanda, 2024). We measure **strict transfer**: the patched target output equals the *source* gold sum (parse failures count as failures).

Table 1 shows a sharp phase transition: early layers are controlled by non-last tokens, while beyond layer 16 the answer becomes overwriteable almost entirely via the last-token residual state.

**Result-writing boundary.** We define the *result-writing boundary* as the depth at which causal control shifts from non-last tokens to the last input token. For Llama-3-8B on three-digit addition under our one-token readout, this boundary is sharply localized to **layer 16**.

Layer range	Last-token strict $\uparrow$	Non-last strict $\uparrow$
0–16	0.00	$\approx 0.99$
17–32	1.00	$\approx 0.00$

Table 1: Cross-sample `resid_post` patching (strict transfer). Early layers are controlled by non-last tokens; after the transition near layer 16, overwriting only the last-token residual transfers the source answer, while overwriting non-last tokens has negligible effect. Full per-layer curves and additional diagnostics appear in Appendix A.

## 4.2 Attention ablation shows attention is dispensable beyond the boundary

Residual patching localizes *where* result semantics live, but does not by itself prove that self-attention is no longer required after the boundary. We therefore perform *cumulative attention ablation*: for a start layer  $s$ , we ablate attention in the suffix  $[s, 32]$  by zeroing the attention-sublayer output in every ablated block, i.e.,  $\text{attn\_out}^{(l)}(t) \leftarrow 0$  for all positions  $t$  and all  $l \in [s, 32]$  (details in Appendix A), leaving the residual connection, MLP, and layer-norm computations unchanged, and evaluate strict accuracy on a held-out set filtered to baseline-correct examples under the same one-token protocol.

Table 2 corroborates the boundary: ablating attention starting at or before layer 16 collapses accuracy, whereas ablating only layers *after* the boundary (start  $s \geq 17$ ) leaves accuracy essentially unchanged. We provide the full accuracy-vs-start-layer curve with confidence intervals in Appendix A.

**Takeaway.** Together, cross-sample patching and cumulative attention ablation establish a clean post-routing last-token regime: **beyond layer 16**, three-digit addition is effectively last-token-only and late computation can be modeled as transformations of the last-token residual stream. Accordingly, all subsequent causal edits operate on the last-token `resid_post` state at layers  $l \geq 17$ , unless otherwise stated.

## 5 Methodology

All experiments operate in the post-routing, last-token regime established in Sec. 4. Our intervention pipeline is: (i) learn simple *functional vectors* from last-token states via diff-of-means (DoM), (ii) when these directions vary with a nuisance context, align context-conditioned *dictio-*

Ablated Layers	Accuracy (%)
None (baseline)	100.0
17–32	$\approx 0.0$
18–32	$\geq 99.9$

Table 2: Accuracy on baseline-correct subset (thus baseline=100%). Strict accuracy after cumulative attention ablation. Attention is causally necessary through the result-writing boundary, but becomes dispensable in the post-routing regime (layers  $\geq 17$ ) under the one-token readout. Full curves and confidence intervals are in Appendix A.

*naries* across contexts using a low-rank orthogonal Procrustes map, and (iii) edit the last-token `resid_post` at a chosen layer and evaluate strict counterfactual success under a one-token readout (Sec. 3). Full implementation details are deferred to Appendix C.

### 5.1 Learning functional vectors (DoM)

Let  $h_{\text{last}}^l \in \mathbb{R}^d$  denote the last-token residual-stream state at layer  $l$ . For a binary attribute  $a$  (e.g., “result hundreds digit equals 7”), we define the unit DoM direction

$$\hat{u}_l^{(a)} = \frac{\mathbb{E}[h_{\text{last}}^l | a] - \mathbb{E}[h_{\text{last}}^l | \neg a]}{\|\mathbb{E}[h_{\text{last}}^l | a] - \mathbb{E}[h_{\text{last}}^l | \neg a]\|_2}. \quad (1)$$

Expectations are estimated by sample averages over synthetic prompts (Sec. 3).

**Within-condition negatives.** When learning directions for values under a fixed nuisance context  $c$  (below), we construct negatives *within the same*  $c$  to prevent the direction from conflating the value with the context itself.

### 5.2 Context-conditioned dictionaries and low-rank alignment

Many digit(-sum) directions are strongly *context-conditioned*: the appropriate direction depends on a nuisance context  $c$  (e.g., next-higher digit context). For discrete contexts  $c \in \mathcal{C}$  and values  $v \in \mathcal{V}$ , we form within-context one-vs-rest DoM directions:

$$u_{c,v}^{(l)} := \frac{\mathbb{E}[h_{\text{last}}^l | c, v] - \mathbb{E}[h_{\text{last}}^l | c, v' \neq v]}{\|\mathbb{E}[h_{\text{last}}^l | c, v] - \mathbb{E}[h_{\text{last}}^l | c, v' \neq v]\|_2}. \quad (2)$$

**Low-rank orthogonal Procrustes (summary).** Stacking  $\{u_{c,v}^{(l)}\}_{v \in \mathcal{V}}$  yields a value-indexed dictionary per context. We compute a rank- $r$  basis for

each context dictionary (e.g., by SVD) and estimate an orthogonal map between the resulting coordinate systems by minimizing a Frobenius alignment loss:

$$R_l^{(c_{\text{ref}} \rightarrow c)} = \arg \min_{R^\top R = I} \left\| \Phi_l^{(c_{\text{ref}})} R - \Phi_l^{(c)} \right\|_F. \quad (3)$$

We then rotate reference-context directions into the target context and use them for editing. We report alignment quality using (i) unaligned value-matched cosine, (ii) Procrustes-aligned cosine, and (iii) a relative reconstruction error; precise definitions and additional controls appear in Appendix C.2.

### 5.3 Vector editing operators

All edits modify  $h_{\text{last}}^l$  at a chosen layer  $l$  and then run the remaining layers unmodified, followed by a greedy one-token readout (Sec. 3). Most experiments use a constant remove-and-add translation:

$$h_{\text{last}}^l = h_{\text{last}}^l - \beta \hat{u}_l^{(a)} + \alpha \hat{u}_l^{(b)}, \quad \alpha, \beta \geq 0, \quad (4)$$

where  $a$  is the source attribute and  $b$  is the target attribute. We also use a norm-calibrated parameterization to make scales comparable across layers/attributes (Appendix C.3).

### 5.4 Hyperparameter selection and reporting protocol

We avoid per-pair tuning by selecting  $(\alpha, \beta)$  on a small *anchor* subset of edit pairs at each layer (and, when relevant, each context/mode) using a fixed discrete grid, then freezing the chosen scales for the full sweep. We evaluate all edit pairs with fixed scales on a held-out set and aggregate using weighted means with weights equal to the number of valid evaluated examples  $n_{\text{total}}$ . For strict success and preservation rates we report Wilson 95% confidence intervals; with multiple random seeds we pool counts across seeds (equivalently weighting by  $n_{\text{total}}$ ).

## 6 Context-Conditioned Rotations of Digit(-Sum) Direction Dictionaries

**Motivation and phenomenon.** Functional directions for a fixed digit(-sum) attribute often fail to transfer under shifts in a *nuisance context* variable (e.g., the next-higher digit context). In the post-routing regime (Sec. 4), we find that this failure is *structured*: for a fixed layer  $L$ , the within-context direction dictionary varies with context,

yet the change is well approximated by an *approximately orthogonal* re-parameterization inside a shared low-rank core. We quantify this using the dictionary alignment protocol and metrics introduced in Appendix C.2, and refer to the resulting structure as *dictionary-level isomorphism across contexts*.

### 6.1 Two digit-shifted settings

We instantiate the context-conditioned dictionary construction in two adjacent digit places. Across settings,  $k$  denotes the *focal digit(-sum) attribute* (either a digit-sum bucket or a digit-value bucket), while  $c$  denotes a *next-higher-digit nuisance context* that shifts the representation but does not change the focal label.

**(i) Ones-sum dictionaries across stripped-tens contexts.** Define the focal ones-sum bucket

$$k := (a \bmod 10) + (b \bmod 10) \in \{0, \dots, 18\}, \quad (5)$$

and the stripped-tens context (pre-carry)

$$c = T := (\lfloor a/10 \rfloor + \lfloor b/10 \rfloor) \bmod 10 \in \{0, \dots, 9\}. \quad (6)$$

Here  $\mathcal{V} = \{0, \dots, 18\}$ .

### 6.2 Results: dictionary-level isomorphism across contexts

**Layerwise summary.** Figure 1 shows a layerwise sweep of cross-context dictionary similarity for both digit-shifted settings, averaging over *off-diagonal* context pairs  $(c_1, c_2)$  with  $c_1 \neq c_2$ . Unaligned similarity  $\text{Cos}_{\text{unaligned}}$  decreases with depth, indicating that individual bucket directions are not invariant under context shifts. However, after low-rank Procrustes alignment (details in Appendix C.2),  $\text{Cos}_{\text{proc}}$  remains near unity while  $\text{RelFro}$  stays small, consistent with an approximately orthogonal re-parameterization inside a shared low-rank core.

**A concrete visual anchor.** Figure 2 shows a representative post-routing layer in the ones-sum setting: unaligned similarity varies substantially across context pairs, whereas Procrustes alignment collapses similarity to near unity, illustrating the same effect at a fixed depth.

**Takeaway and causal prediction.** This section establishes a structured geometric claim: digit(-sum) direction dictionaries vary with nuisance

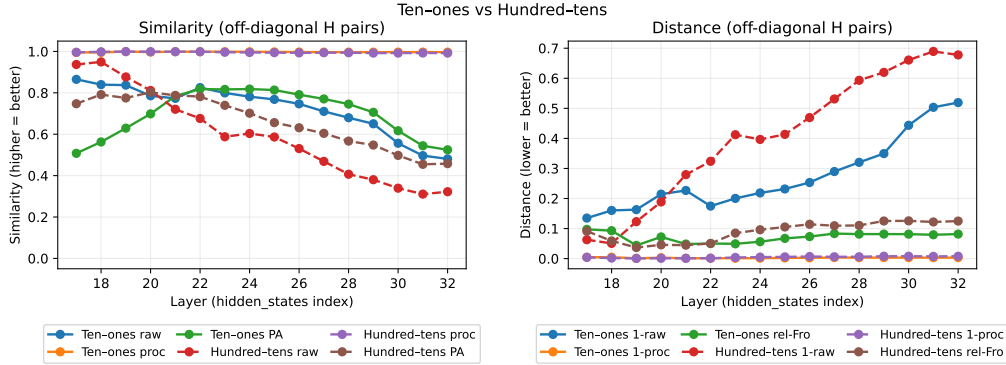


Figure 1: **Layerwise context-conditioned dictionary isomorphism (two digit-shifted settings)**. For each layer  $L$ , metrics are averaged over off-diagonal context pairs  $(c_1, c_2)$ . **(a)** Unaligned cosine decreases with depth, indicating non-invariance of individual bucket directions. **(b)** After low-rank orthogonal Procrustes alignment (Sec. C.2), aligned cosine remains near unity while RelFro stays small, consistent with a rotation-like re-parameterization of a shared low-rank core. Solid: stripped-tens context  $\rightarrow$  ones-sum; dashed: result-hundreds-digit context  $\rightarrow$  result-tens digit.

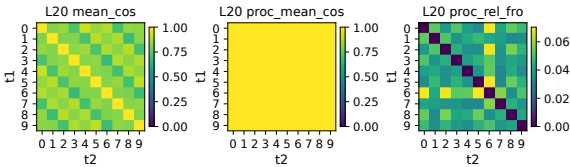


Figure 2: **Single-layer anchor: context-conditioned rotation at a fixed depth**. At a representative post-routing layer, unaligned similarity between context dictionaries varies substantially (top), while low-rank Procrustes alignment collapses similarity to near unity (bottom).

context, yet are related by an approximately orthogonal change of coordinates in a shared low-rank core. In the next section (Sec. 7.2), we test the corresponding *causal prediction*: directions learned under one context should fail when applied under a shifted context (TRANSFER), but should recover after applying the learned rotator (ROTATED), while negative controls should not recover.

## 7 One-Dimensional Result-Digit Editing Axes

We now give a causal test of the context-conditioned rotation claim (Sec. 6) in the post-routing last-token regime (Sec. 4).

The operational prediction is simple: directions learned under one nuisance context typically fail to edit under a shifted context (TRANSFER), but should recover after applying the learned low-rank rotator (ROTATED), approaching the within-context upper bound (DIRECT); negative controls

should not recover. All interventions modify last-token `resid_post` at layer  $l$  and are evaluated by strict numeric counterfactuals under the one-token readout (Sec. 3).

### 7.1 Setup: strict counterfactual targets, diagnostics, and modes

**Digit edit objective.** Let  $s = a + b = 100h + 10x + y$  be the gold three-digit sum. A digit edit selects a place  $p \in \{\text{HUNDREDS}, \text{TENS}, \text{ONES}\}$  and a value change  $(v \rightarrow v')$  at that place. We allow carry/borrow propagation and define the strict target by the induced numeric offset:

$$\Delta(p; v \rightarrow v') = (v' - v) \cdot 10^{k(p)},$$

$$k(\text{HUNDREDS}) = 2, \quad k(\text{TENS}) = 1, \quad k(\text{ONES}) = 0,$$

$$s_{\text{cf}} = s + \Delta(p; v \rightarrow v'). \quad (7)$$

We report **strict** success iff the decoded integer equals  $s_{\text{cf}}$  (parse failures count as failures).

**Illustrative example (tens-digit edit).** Consider an instance whose baseline decoded (gold) sum is the three-digit integer  $s = 423$ , so  $(h, x, y) = (4, 2, 3)$ . We choose place  $p = \text{TENS}$  and value change  $(v \rightarrow v') = (2 \rightarrow 5)$ . By Eq. (7), the induced offset is  $\Delta = (5 - 2) \cdot 10 = 30$ , hence the strict counterfactual target is  $s_{\text{cf}} = 423 + 30 = 453$  (no carry/borrow occurs in this example).

At a post-routing layer  $l$ , let  $h_{\text{last}}^l$  denote the last-token `resid_post` state for this prompt. Let  $\hat{u}_l^{(H=4, t=2)}$  and  $\hat{u}_l^{(H=4, t=5)}$  be the unit DoM directions for the TENS digit value  $t \in \{2, 5\}$  under the hundreds-digit context  $H = 4$  (Eq. (2)).

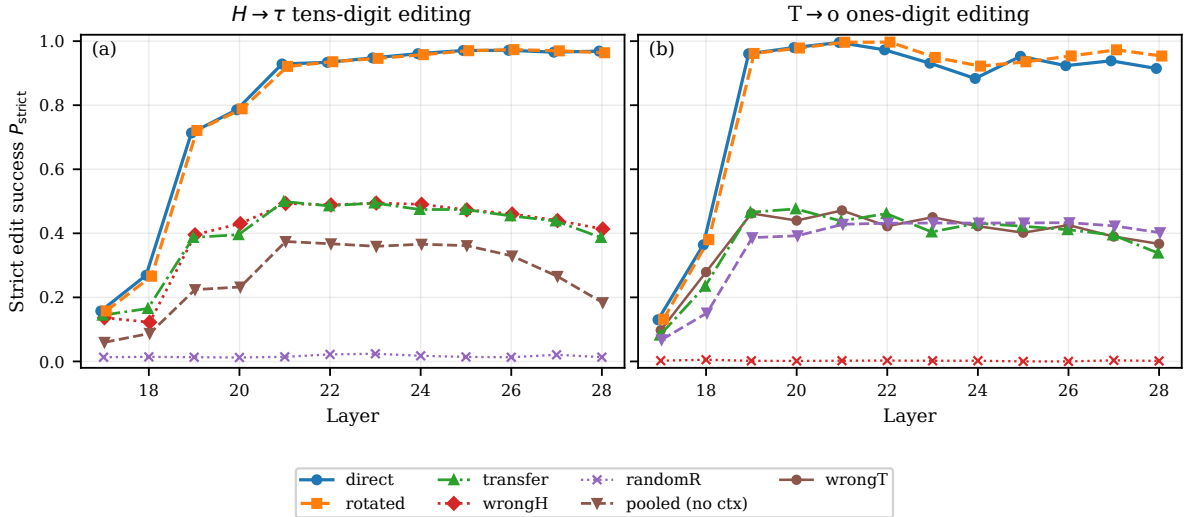


Figure 3: **Rotation is necessary for cross-context digit editing.** Strict counterfactual success vs. layer (baseline-correct subset). ROTATED recovers toward DIRECT, while TRANSFER collapses; WRONG-CONDITION and RANDOM- $R$  fail to recover.

We apply the remove-and-add edit (Eq. (4)):

$$h_{\text{last}}^l = h_{\text{last}}^l - \beta \hat{u}_l^{(H=4, t=2)} + \alpha \hat{u}_l^{(H=4, t=5)}, \quad (8)$$

$$\alpha, \beta \geq 0,$$

then run the remaining blocks unmodified and decode with the one-token readout. We expect this intervention to causally shift the model’s decoded output from 423 to 453, i.e., replacing the tens digit “2” with “5” while preserving the hundreds and ones digits.

**Diagnostics.** In addition to strict success, we report (i) **parse rate** and (ii) non-target digit preservation:  $\text{Preserve}_{-p} = 1$  iff the two non-target digits match  $(h, x, y)$ .

**Modes and controls.** We compare: DIRECT (learn+edit within the eval context), TRANSFER (reuse a source-context direction without adjustment), ROTATED (rotate the source direction into the eval context; Sec. C.2). Controls are WRONG-CONDITION (mismatched rotator) and RANDOM- $R$  (random orthogonal map at the same rank), ruling out “any rotation works” explanations.

## 7.2 Main causal test: rotation enables cross-context digit editing

We evaluate two context-shifted settings aligned with Sec. 6.1: (i) ones-digit editing under stripped-tens context shifts ( $T$ ), and (ii) tens-digit editing under hundreds-context shifts ( $H$ ). At layer  $l$ , we learn within-context value directions (Eq. 2),

estimate rank- $r$  Procrustes rotators between contexts (Sec. C.2), and apply the same remove-and-add edit operator (Eq. 4) using either direct, transferred, or rotated directions. Figure 3 shows the predicted pattern: TRANSFER collapses under context shift, while ROTATED largely restores strict success toward DIRECT; controls do not recover.

**Edit-magnitude sensitivity.** To stress-test cross-context failure, we stratify by  $|\Delta| = |v' - v|$  (larger edits induce more carry interactions). Figure 4 aggregates strict success over representative post-routing layers (24–26): TRANSFER degrades sharply with  $|\Delta|$ , while ROTATED tracks DIRECT; RANDOM- $R$  remains near chance.

## 7.3 Cross-prompt transport of digit-editing interventions

To test whether the learned directions encode result-digit semantics rather than template-specific artifacts, we learn all directions (and rotators, when applicable) from a single canonical template: “Calculate: {a}+{b} = ”. We then apply the same last-token interventions under three alternative paraphrases.

As shown in Fig. 5, Prompt1 and Prompt3 yield curves close to the origin, whereas Prompt2 is markedly worse; we view this as an interesting extension and do not further analyze prompt-sensitivity in this section.

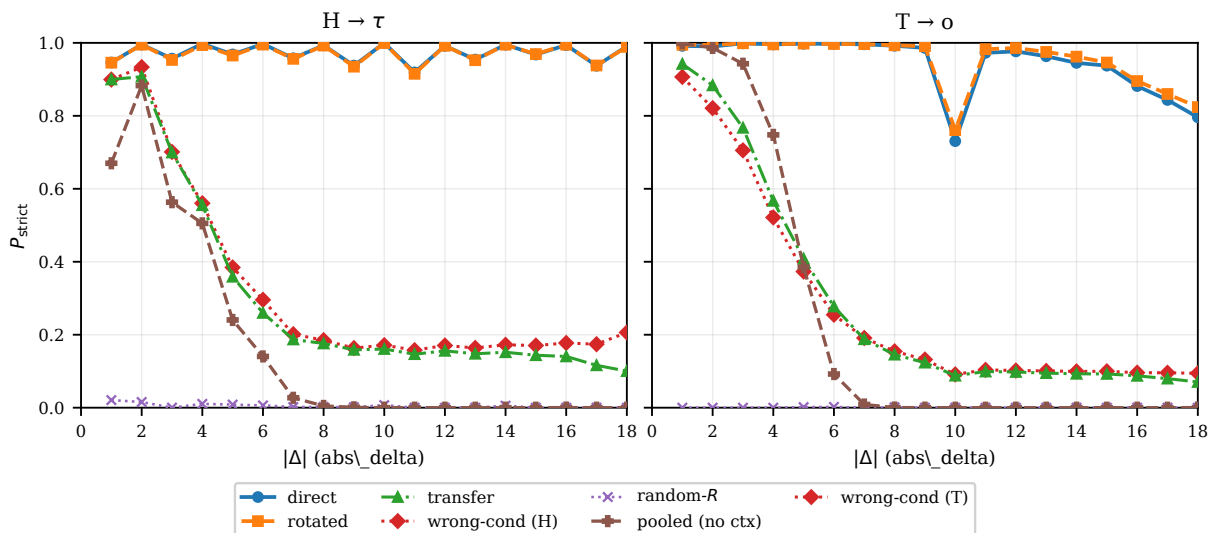


Figure 4: **Edit-magnitude sensitivity across two settings.** Strict success vs.  $|\Delta|$  (layers 24–26, weighted by  $n_{\text{total}}$ ). Left:  $H \rightarrow t$ . Right:  $T \rightarrow o$ . TRANSFER degrades with  $|\Delta|$ , while ROTATED remains close to DIRECT; RANDOM-R and wrong-condition controls do not recover.

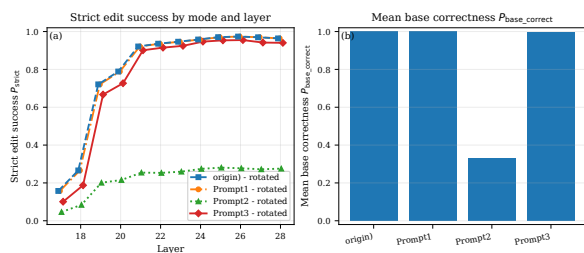


Figure 5: Cross-prompt transport of digit-editing interventions. **(a)** Strict edit success vs. layer under the canonical template and three paraphrases. **(b)** Right: bar plot of answer accuracy under each prompt.

## 7.4 Takeaway

In the post-routing last-token regime, individual result digits admit near one-dimensional causal control: (i) within-context digit edits succeed under strict numeric counterfactual evaluation, (ii) cross-context reuse fails in a structured way, and (iii) the learned low-rank rotation restores editability, while negative controls do not. Together with cross-prompt transport, these results support interpreting the learned directions as task-semantic result-digit representations in the last-token residual stream.

## 8 Limitations

- **Task and readout specificity.** Our findings are established for three-digit base-10 addition in a single model (Meta-Llama-3-

8B, base) under a deliberately constrained *one-token* numeric readout. The location and sharpness of the result-writing boundary, as well as the post-routing “last-token-only” behavior, may change for other arithmetic tasks (e.g., subtraction/multiplication), longer numbers, different tokenizers, or multi-token generation where later tokens can re-introduce routing dependencies.

- **Partial mechanistic coverage.** We focus on late-stage answer finalization *after* cross-token routing becomes causally irrelevant. Our methods do not provide a full end-to-end explanation of how earlier layers compute carries and intermediate representations, nor do they fully characterize the circuits that route information into the last token before the boundary.
- **Intervention class limitations.** Our causal edits rely on simple diff-of-means functional vectors and low-rank orthogonal alignment. These tools may miss nonlinear structure, multi-direction interactions, or cases where the relevant subspace is not well-approximated by a shared low-rank core. Similarly, “rotation-like” alignment is an approximation and may break under harder distribution shifts.
- **Broader replication.** We do not yet know

how these phenomena vary across model families, scales, training recipes, or fine-tuned/chat variants. Cross-model replication and systematic comparisons are required before treating the boundary and the low-rank alignment structure as general properties of decoder-only LLMs.

## 9 Conclusion

We presented a causal and geometric account of how Meta-Llama-3-8B (base) finalizes three-digit addition once cross-token routing ceases to matter. Using a one-token readout, cross-sample residual patching localizes a sharp result-writing boundary near layer 17, where causal control of the decoded sum shifts from non-last tokens to the last input token. Complementary cumulative attention ablations indicate that, beyond this boundary, late-layer self-attention is largely dispensable, supporting a post-routing picture in which computation is dominated by MLP-mediated updates to the last-token residual stream.

Within this post-routing regime, we find that digit(-sum) functional directions are strongly context-conditioned but structured: dictionaries learned under different next-higher-digit contexts are well-related by an approximately orthogonal re-parameterization inside a shared low-rank core, captured by low-rank Procrustes alignment. We then causally validate the corresponding prediction in digit editing: direct within-context edits succeed, naive cross-context transfer collapses, and rotating directions through the learned alignment largely restores strict counterfactual performance, while negative controls fail to recover. Together, these results support a mechanistic view in which the model writes arithmetic results into the last token after routing ends, and the relevant representations transform predictably across nuisance-context shifts.

A natural next step is to extend this framework beyond three-digit addition and beyond the specific one-token readout, and to map the low-rank aligned subspaces to more explicit circuit components.

## References

- Anthropic. 2025. Tracing the thoughts of a large language model. <https://www.anthropic.com/research/tracing-thoughts-language-model>. Anthropic Research (online article).
- Andy Arditi, Oscar Obeso, Aaqib Syed, Daniel Paleka, Nina Panickssery, Wes Gurnee, and Neel Nanda. 2024. [Refusal in language models is mediated by a single direction](#). In *Advances in Neural Information Processing Systems 38: Annual Conference on Neural Information Processing Systems 2024, NeurIPS 2024, Vancouver, BC, Canada, December 10 - 15, 2024*.
- Yonatan Belinkov. 2022. [Probing classifiers: Promises, shortcomings, and advances](#). *Comput. Linguistics*, 48(1):207–219.
- Lawrence Chan, Adria Garriga-Alonso, Nicholas Goldowsky-Dill, Ryan Greenblatt, Jenny Nitishinskaya, Ansh Radhakrishnan, Buck Shlegeris, and Nate Thomas. 2022. Causal scrubbing: A method for rigorously testing interpretability hypotheses. In *AI Alignment Forum*, volume 2.
- Abhimanyu Dubey, Abhinav Jauhri, Abhinav Pandey, Abhishek Kadian, Ahmad Al-Dahle, Aiesha Letman, Akhil Mathur, Alan Schelten, Amy Yang, Angela Fan, et al. 2024. The llama 3 herd of models. *arXiv e-prints*, pages arXiv–2407.
- Stefan Heimersheim and Neel Nanda. 2024. [How to use and interpret activation patching](#). *CoRR*, abs/2404.15255.
- Jorrit Kruthoff. 2024. [Carrying over algorithm in transformers](#).
- Jack Lindsey et al. 2025. On the biology of a large language model. <https://transformer-circuits.pub/2025/attribution-graphs/biology.html>. Transformer Circuits Thread (online paper).
- Siddarth Mamidanna, Daking Rai, Ziyu Yao, and Yilun Zhou. 2025. [All for one: LLMs solve mental math at the last token with information transferred from other tokens](#). In *Proceedings of the 2025 Conference on Empirical Methods in Natural Language Processing*, pages 30735–30748, Suzhou, China. Association for Computational Linguistics.
- Kevin Meng, David Bau, Alex Andonian, and Yonatan Belinkov. 2022. [Locating and editing factual associations in GPT](#). In *Advances*

in *Neural Information Processing Systems 35: Annual Conference on Neural Information Processing Systems 2022, NeurIPS 2022, New Orleans, LA, USA, November 28 - December 9, 2022*.

Neel Nanda, Lawrence Chan, Tom Lieberum, Jess Smith, and Jacob Steinhardt. 2023. [Progress measures for grokking via mechanistic interpretability](#). In *The Eleventh International Conference on Learning Representations*.

Yaniv Nikankin, Anja Reusch, Aaron Mueller, and Yonatan Belinkov. 2025. [Arithmetic without algorithms: Language models solve math with a bag of heuristics](#). In *The Thirteenth International Conference on Learning Representations, ICLR 2025, Singapore, April 24-28, 2025*. OpenReview.net.

Philip Quirke and Fazl Barez. 2024. [Understanding addition in transformers](#). In *The Twelfth International Conference on Learning Representations*.

Alessandro Stolfo, Yonatan Belinkov, and Mrinmaya Sachan. 2023. [A mechanistic interpretation of arithmetic reasoning in language models using causal mediation analysis](#). In *Proceedings of the 2023 Conference on Empirical Methods in Natural Language Processing, EMNLP 2023, Singapore, December 6-10, 2023*, pages 7035–7052. Association for Computational Linguistics.

Fred Zhang and Neel Nanda. 2024. [Towards best practices of activation patching in language models: Metrics and methods](#). In *The Twelfth International Conference on Learning Representations, ICLR 2024, Vienna, Austria, May 7-11, 2024*. OpenReview.net.

Tianyi Zhou, Deqing Fu, Vatsal Sharan, and Robin Jia. 2024. [Pre-trained large language models use fourier features to compute addition](#). In *Advances in Neural Information Processing Systems 38: Annual Conference on Neural Information Processing Systems 2024, NeurIPS 2024, Vancouver, BC, Canada, December 10 - 15, 2024*.

Fangwei Zhu, Damai Dai, and Zhifang Sui. 2025. [Language models encode the value of numbers](#)

[linearly](#). In *Proceedings of the 31st International Conference on Computational Linguistics, COLING 2025, Abu Dhabi, UAE, January 19-24, 2025*, pages 693–709. Association for Computational Linguistics.

## A Details for causal localization (patching and attention ablation)

We provide the exact interventions and the full curves referenced in Sec. 4.

**Setup and filtering.** We use the prompt "Calculate: {a}+{b} = " with a trailing space and the shared one-token parsing protocol (Sec. 3). For cross-sample patching, we form source–target pairs with distinct gold sums and filter to pairs where the unmodified model is baseline-correct on *both* prompts (to avoid confounding from baseline errors).

**Cross-sample patching (exact definition).** Let  $X = (x_1, \dots, x_S)$  be the tokenized prompt and  $\mathbf{r}^{(L)}(X) \in \mathbb{R}^{S \times d}$  be `resid_post` at layer  $L$ . Given  $(X_{\text{src}}, X_{\text{tgt}})$ , we cache  $\mathbf{r}^{(L)}(X_{\text{src}})$  and re-run  $X_{\text{tgt}}$  while overwriting either:

$$\text{Last-token patch: } \mathbf{r}_S^{(L)}(X_{\text{tgt}}) \leftarrow \mathbf{r}_S^{(L)}(X_{\text{src}}), \quad (9)$$

$$\text{Non-last patch: } \mathbf{r}_i^{(L)}(X_{\text{tgt}}) \leftarrow \mathbf{r}_i^{(L)}(X_{\text{src}}), \quad (10)$$

for  $i = 1, \dots, S - 1$ .

We then run layers  $L+1, \dots, 31$  normally and decode one token. **Strict transfer** counts success iff the parsed output equals  $s_{\text{src}}$  (parse failures are failures).

**Cumulative attention ablation and uncertainty.** For a start layer  $s$ , we ablate attention outputs in all blocks  $l \in [s, 31]$  (MLP and residual path intact), then decode with the same one-token protocol. We evaluate strict accuracy on a held-out set filtered to baseline-correct examples. When using multiple seeds, we pool counts and report Wilson 95% confidence intervals.

Layer	ones-sum dict (stripped-tens)			tens-sum dict (stripped-hundreds)		
	Unaligned	Procrustes	RelFro	Unaligned	Procrustes	RelFro
17	0.94 ± 0.02	1.00 ± 0.00	0.09	0.87 ± 0.10	1.00 ± 0.00	0.10
18	0.95 ± 0.02	1.00 ± 0.00	0.06	0.84 ± 0.19	1.00 ± 0.00	0.09
19	0.88 ± 0.08	1.00 ± 0.00	0.04	0.84 ± 0.11	1.00 ± 0.00	0.04
20	0.81 ± 0.14	1.00 ± 0.00	0.04	0.79 ± 0.26	1.00 ± 0.00	0.07
21	0.72 ± 0.21	1.00 ± 0.00	0.05	0.77 ± 0.15	1.00 ± 0.00	0.05
22	0.68 ± 0.21	1.00 ± 0.00	0.05	0.83 ± 0.11	1.00 ± 0.00	0.05
23	0.59 ± 0.27	1.00 ± 0.01	0.08	0.80 ± 0.11	1.00 ± 0.00	0.05
24	0.60 ± 0.20	0.99 ± 0.01	0.10	0.78 ± 0.08	1.00 ± 0.00	0.06
25	0.59 ± 0.16	0.99 ± 0.00	0.11	0.77 ± 0.07	1.00 ± 0.00	0.07
26	0.53 ± 0.20	0.99 ± 0.01	0.11	0.75 ± 0.06	1.00 ± 0.00	0.07
27	0.47 ± 0.17	0.99 ± 0.00	0.11	0.71 ± 0.07	1.00 ± 0.00	0.08
28	0.41 ± 0.18	0.99 ± 0.00	0.11	0.68 ± 0.07	1.00 ± 0.00	0.08

Table 3: **Full layerwise summary for digit-sum dictionary rotations.** Mean±std over context pairs for unaligned ( $k$ -aligned) cosine and Procrustes-aligned cosine, along with relative Frobenius reconstruction error (RelFro), reported for layers  $L \in [17, 28]$  in the ones-sum (stripped-tens context) and tens-sum (stripped-hundreds context) settings.

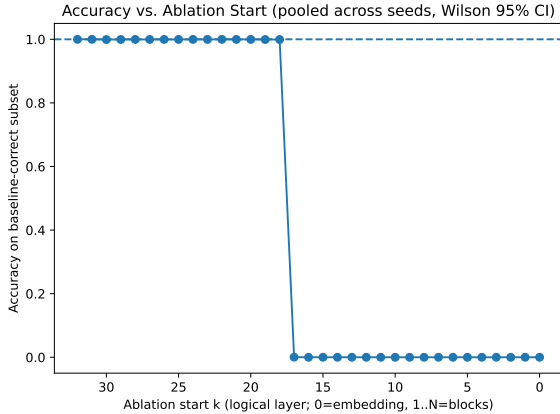


Figure 6: **Cross-sample patching curves.** Strict transfer vs. layer for last-token and non-last patching on baseline-correct source–target pairs. A sharp crossover occurs near layer 16.

## B Additional Results for Digit-Sum Dictionary Rotations

### B.1 Full layerwise summary tables

### C Additional Method Details

This appendix provides mathematical and implementation details for the methodology in Sec. 5, including conditional dictionary construction, low-rank orthogonal alignment, rotated transfer, control modes, and norm-calibrated editing.

#### C.1 DoM estimation details

We estimate expectations in Eqs. (1) and (2) by sample averages over synthetic prompts (Sec. 3).

For conditional directions we always use within-condition negatives (i.e., negatives share the same context  $c$ ) to avoid conflating value with context.

### C.2 Conditional dictionaries and low-rank orthogonal alignment

**Conditional attributes.** Let  $c \in \mathcal{C}$  denote a condition/domain variable and  $v \in \mathcal{V}$  denote the edited attribute value. At layer  $l$ , define the conditional DoM direction (one-vs-rest within fixed  $c$ ):

$$u_l^{(c,v)} := \mathbb{E}[h_{\text{last}}^l | c, v] - \mathbb{E}[h_{\text{last}}^l | c, v' \in \mathcal{V} \setminus \{v\}],$$

$$\hat{u}_l^{(c,v)} := \frac{u_l^{(c,v)}}{\|u_l^{(c,v)}\|_2}.$$
(11)

**Row matrices for alignment.** For each condition  $c$ , stack row-normalized directions across values  $v$ :

$$U_l^{(c)} := [\hat{u}_l^{(c,v)}]_{v \in \mathcal{V}} \in \mathbb{R}^{|\mathcal{V}| \times d}. \quad (12)$$

**Low-rank bases.** To avoid estimating a full  $d \times d$  rotation, we compute a rank- $r$  orthonormal basis  $B_l^{(c)} \in \mathbb{R}^{d \times r}$  for each condition (e.g., by taking the top- $r$  right singular vectors of  $U_l^{(c)}$ ).

We denote the coordinates of a direction in this basis by

$$\phi_l^{(c,v)} := \hat{u}_l^{(c,v)} B_l^{(c)} \in \mathbb{R}^r,$$

$$\Phi_l^{(c)} := U_l^{(c)} B_l^{(c)} \in \mathbb{R}^{|\mathcal{V}| \times r}. \quad (13)$$

**Orthogonal Procrustes rotators.** Given a reference condition  $c_{\text{ref}}$  and an evaluation condition  $c$ , we estimate an orthogonal matrix  $R_l^{(c_{\text{ref}} \rightarrow c)} \in \mathbb{R}^{r \times r}$  by

$$R_l^{(c_{\text{ref}} \rightarrow c)} := \arg \min_{R^\top R = I} \left\| \Phi_l^{(c_{\text{ref}})} R - \Phi_l^{(c)} \right\|_F. \quad (14)$$

In practice this is solved via the SVD of  $(\Phi_l^{(c_{\text{ref}})})^\top \Phi_l^{(c)}$ .

**Rotated transfer of functional directions.** To transfer an attribute direction learned under  $c_{\text{ref}}$  to condition  $c$ , we map it through aligned low-rank subspaces:

$$\begin{aligned} z_l^{(c_{\text{ref}}, v)} &:= (B_l^{(c_{\text{ref}})})^\top \hat{u}_l^{(c_{\text{ref}}, v)} \in \mathbb{R}^r, \\ \bar{u}_l^{(c \leftarrow c_{\text{ref}}, v)} &:= B_l^{(c)} R_l^{(c_{\text{ref}} \rightarrow c)} z_l^{(c_{\text{ref}}, v)} \in \mathbb{R}^d, \\ \tilde{u}_l^{(c \leftarrow c_{\text{ref}}, v)} &:= \frac{\bar{u}_l^{(c \leftarrow c_{\text{ref}}, v)}}{\left\| \bar{u}_l^{(c \leftarrow c_{\text{ref}}, v)} \right\|_2} \in \mathbb{R}^d. \end{aligned} \quad (15)$$

We use  $\tilde{u}$  in the same editing operators as direct directions.

**Control modes.** We report multiple modes that isolate direction quality versus alignment quality:

- **direct:** use  $\hat{u}_l^{(c, v)}$  learned under the evaluation condition  $c$ .
- **transfer:** use  $\hat{u}_l^{(c_{\text{ref}}, v)}$  directly without rotation.
- **rotated:** use  $\tilde{u}_l^{(c \leftarrow c_{\text{ref}}, v)}$  from Eq. (15).
- **wrong-condition:** rotate using  $R_l^{(c_{\text{ref}} \rightarrow c_{\text{wrong}})}$  for some  $c_{\text{wrong}} \neq c$ .
- **random- $R$ :** rotate using a random orthogonal matrix in  $\mathbb{R}^{r \times r}$ .

### C.3 Editing operators and scale calibration

**Additive steering.** Given a unit direction  $\hat{u}_l^{(a)}$  and scalar  $\alpha \in \mathbb{R}$ ,

$$h'_{\text{last}} = h_{\text{last}}^l + \alpha \hat{u}_l^{(a)}. \quad (16)$$

**Constant remove-and-add editing.** Given attributes  $a$  (source) and  $b$  (target),

$$h'_{\text{last}} = h_{\text{last}}^l - \beta \hat{u}_l^{(a)} + \alpha \hat{u}_l^{(b)}, \quad \alpha, \beta \geq 0. \quad (17)$$

**Norm-calibrated parameterization.** To improve comparability of scale parameters across layers/attributes, we also use

$$h'_{\text{last}} = h_{\text{last}}^l - \beta_s \|r_l^{(a)}\|_2 \hat{u}_l^{(a)} + \alpha_s \|r_l^{(b)}\|_2 \hat{u}_l^{(b)}, \quad (18)$$

where  $\alpha_s, \beta_s$  are dimensionless scales and  $r_l^{(a)}, r_l^{(b)}$  denote the corresponding (unnormalized) DoM vectors before unit normalization.

### Hyperparameter selection (implementation).

Unless otherwise stated, we sweep a small grid of norm-calibrated scales  $\alpha_s, \beta_s \in \{0.5, 1.0\}$ , select the best-performing pair on a small anchor subset, and then evaluate with fixed scales on a larger set. We always report baseline (no-intervention) performance under the same parsing and strict metrics.

### C.4 Exact cross-context dictionary metrics

Fix layer  $l$ . For each context  $c$ , stack unit directions over values to form a dictionary

$$U_c^{(l)} := \begin{bmatrix} u_{c, v_1}^{(l)} \\ \vdots \\ u_{c, v_{|\mathcal{V}|}}^{(l)} \end{bmatrix} \in \mathbb{R}^{|\mathcal{V}| \times d}. \quad (19)$$

**Unaligned cosine.** For a context pair  $(c_1, c_2)$ ,

$$\text{Cos}_{\text{unaligned}}(c_1, c_2) = \frac{1}{|\mathcal{V}|} \sum_{v \in \mathcal{V}} \langle u_{c_1, v}^{(l)}, u_{c_2, v}^{(l)} \rangle. \quad (20)$$

**Low-rank Procrustes alignment.** Let  $B_c^{(l)} \in \mathbb{R}^{d \times r}$  be the top- $r$  right singular vectors of  $U_c^{(l)}$  and define  $X_c^{(l)} = U_c^{(l)} B_c^{(l)} \in \mathbb{R}^{|\mathcal{V}| \times r}$ . For  $(c_1, c_2)$ , solve

$$R_{c_1 \rightarrow c_2}^{(l)} = \arg \min_{R^\top R = I} \left\| X_{c_1}^{(l)} R - X_{c_2}^{(l)} \right\|_F, \quad (21)$$

and reconstruct an aligned dictionary in  $c_2$ 's ambient coordinates:

$$U_{c_1 \rightarrow c_2}^{(l)} = \left( U_{c_1}^{(l)} B_{c_1}^{(l)} \right) R_{c_1 \rightarrow c_2}^{(l)} \left( B_{c_2}^{(l)} \right)^\top. \quad (22)$$

Row-normalize  $U_{c_1 \rightarrow c_2}^{(l)}$  before cosine computation.

**Aligned cosine and reconstruction error.** Let  $\tilde{u}_{c_1 \rightarrow c_2, v}^{(l)}$  be the row-normalized  $v$ -th row of

$U_{c_1 \rightarrow c_2}^{(l)}$ . Then

$$\text{Cos}_{\text{proc}}(c_1, c_2) = \frac{1}{|\mathcal{V}|} \sum_{v \in \mathcal{V}} \langle \tilde{u}_{c_1 \rightarrow c_2, v}^{(l)}, u_{c_2, v}^{(l)} \rangle, \quad (23)$$

$$\text{RelFro}(c_1, c_2) = \frac{\|U_{c_1 \rightarrow c_2}^{(l)} - U_{c_2}^{(l)}\|_F}{\|U_{c_2}^{(l)}\|_F}. \quad (24)$$

**Averaging over context pairs.** For layerwise summaries, we average each metric over off-diagonal context pairs  $(c_1, c_2)$  with  $c_1 \neq c_2$ .